Super-selective Removal of Lead from Water by Two-Dimensional MoS_2 Nanosheets and Layer-stacked Membranes

Research article

Revision Submitted to

Environmental Science & Technology

Zhongying Wang,[1,2]*# Qingsong Tu[3#], Alison Sim[1], Julie Yu[1], Yanghua Duan[1], Sidney Yat-Yin Poon[1], Bei Liu[2], Qi Han[2], Jeffrey J. Urban[4], David Sedlak[1], and Baoxia Mi[1]*

[1]Department of Civil and Environmental Engineering, University of California, Berkeley, California 94720, United States

[2] Guangdong Provincial Key Laboratory of Soil and Groundwater Pollution Control, School of Environmental Science and Engineering, Southern University of Science and Technology, 1088 Xueyuan Blvd, Nanshan District, Shenzhen 518055, PR China

[3]Materials Sciences Division, Lawrence Berkeley National Laboratory, Berkeley, California 94720, United States

[4]The Molecular Foundry, Lawrence Berkeley National Laboratory, Berkeley, California 94720, United States

*The author to whom correspondence should be addressed.

[#] The author contributed equally to the work.

E-mail: mib@berkeley.edu; wangzy6@sustech.edu.cn

Abstract

Point-of-use (POU) devices with satisfactory lead (Pb^{2+}) removal performance are urgently needed in response to recent outbreaks of lead contamination in drinking water. This study experimentally demonstrated the excellent lead removal capability of two-dimensional (2D) MoS_2 nanosheets in aqueous form and as part of a layer-stacked membrane. Among all materials ever reported in the literature, MoS_2 nanosheets exhibit the highest adsorption capacity (740 mg/g), and the strongest selectivity/affinity towards Pb^{2+} with a distribution coefficient K_d that is orders of magnitude higher than that of other lead adsorption materials (5.2×10^7 mL/g). Density functional theory (DFT) simulation was performed to complement experimental measurements and to help understand the adsorption mechanisms. The results confirmed that the cation selectivity of MoS_2 follows the order $Pb^{2+} > Cu^{2+} >> Cd^{2+} > Zn^{2+}$, $Ni^{2+} > Mg^{2+}$, K^+, Ca^{2+}. The membrane formed with layer-stacked MoS_2 nanosheets exhibited a high water flux (145 L/ m^2/h/bar), while effectively decreasing Pb^{2+} concentration in drinking water from a few mg/L to less than 10 μg/L. The removal capacity of the MoS_2 membrane is a few orders of magnitude higher than that of other literature-reported membrane filters. Therefore, the layer-stacked MoS_2 membrane has great potential for POU removal of lead from drinking water.

KEYWORDS: layer-stacked MoS_2 membrane; point-of-use device; lead contamination; drinking water; super-selective adsorption; high adsorption capacity

Table of Contents (TOC)

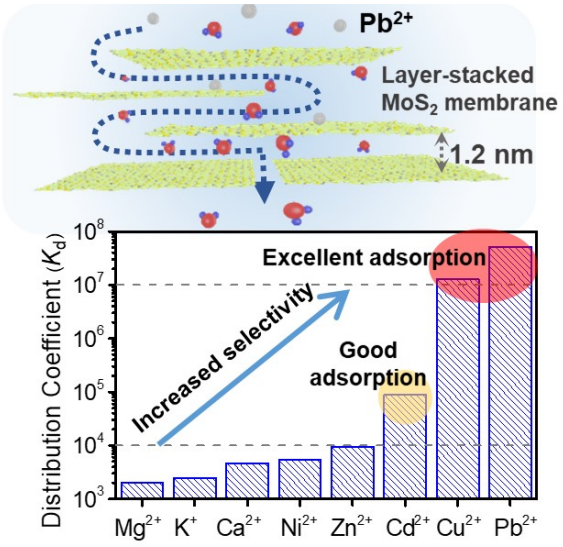

INTRODUCTION

Toxic heavy metal contamination of freshwater and drinking water has become a critical challenge for human society. Particularly, lead (Pb^{2+}) has been recognized as one of the most toxic metals worldwide and there have been cases of lead contamination of tap water in various cities (e.g., Washington, DC; Flint, MI; and Newark, NJ) in the United States. A major source of lead in drinking water is the lead-containing plumbing in water distribution systems like pipes, solders, and fittings. As aged lead-containing pipelines are still used, lead concentrations can be on the order of tens of milligrams per liter in the aftermath of man-made mismanagement or natural disasters.[1, 2] This is several orders of magnitude higher than the U.S. EPA lead action level (15 μg/L) and the WHO guideline value (10 μg/L).[3, 4] Long-term exposure to lead, even at extremely low concentrations, increases the blood lead level due to its bio-accumulative nature, causing severe adverse health effects in the nervous system and brain, particularly in infants and children.[5]

To remove lead from drinking water, especially for daily-use in rural areas or for responding to emergency lead contamination incidents, portable point-of-use (POU) adsorption technologies are essential because of their flexibility, ease of operation, and cost effectiveness. Some promising adsorbents targeting heavy metal remediation have been recently identified, including metal–organic frameworks (MOFs),[6, 7] graphene-based materials,[8] covalent organic frameworks,[9, 10] layered nanomaterials[11-14], and natural materials like biochar[15]. However, sorption materials that have ultrahigh affinity and selectivity to lead are still lacking. High selectivity is extremely important because one challenge hindering effective removal of lead from drinking water is the presence of interfering species. In addition, the adsorption materials used in POU applications should possess attributes such as high porosity, adsorption-site accessibility, and

67 homogeneous binding sites to achieve fast kinetics and high capacity.

68 Two-dimensional (2D) molybdenum disulfide (MoS_2), one of the most widely researched
69 transition metal dichalcogenides (TMDs), is an ideal adsorbent material for heavy metal
70 remediation because of its large surface area, and is abundant active sulfur sites that have a high
71 affinity to heavy metals.[16, 17] Although MoS_2 is a naturally occurring mineral, the direct use of
72 bulk MoS_2 in heavy metal remediation is impossible because the interlayer spacing (0.63 nm) is
73 so small that targeted heavy metal ions are unable to access the interior sulfur atoms. Synthetic
74 2D MoS_2 nanomaterials (*e.g.*, flower-like aggregates) have been explored as adsorbents for toxic
75 transition metal (Hg^{2+}, Pb^{2+}, Ag^{+}, Zn^{2+}, Cd^{2+}) remediation, showing moderate-to-high adsorption
76 capacities[18-25]. However, little investigation has been done to quantify the affinity and selectivity
77 of MoS_2-based adsorbents.[26] The surface area of MoS_2 available for adsorption is also
78 compromised due to the aggregation of MoS_2 nanosheets during hydrothermal synthesis. In
79 contrast, the exfoliated MoS_2 monolayers possess the highest theoretical surface area. However,
80 limited work has been done investigating its application as an adsorbent in a POU device for lead
81 ion removal.

82 To address the above research needs, we systematically studied the adsorption of Pb^{2+} by
83 MoS_2 monolayers and the effects of interfering ions and compared its selectivity and capacity to
84 that of other heavy metal ions. Batch tests and DFT simulations were used to unveil the
85 selectivity and adsorption mechanisms of MoS_2 towards various ions. The layer-stacked MoS_2
86 structure with confined and ordered nanochannels was employed as a POU filter, and its
87 performance and mechanism for removing Pb in continuous filtration was investigated to reveal
88 the potential in practical applications.

89

MATERIALS AND METHODS

MoS_2 monolayer and membrane preparation. To prepare chemically exfoliated monolayer MoS_2 nanosheets,[27] 5 ml of 1.6 M n-butyllithium in hexane solution was added to ~500 mg of bulk MoS_2 powder (~ 2 μm, Sigma-Aldrich), and the mixture was was kept at room temperature for 2 d in a nitrogen-filled glovebox with mild stirring. The resulting lithium-intercalated product was rinsed with hexane to remove organic reactants and by-products. The purified intercalated product was immediately exfoliated by reaction with DI water in an ultrasonic bath for 1 h. MoS_2 nanosheets well-dispersed in solution were obtained after dialysis of the dispersion against DI water to remove inorganic byproduct LiOH. The total MoS_2 concentration was determined through digestion in 0.2 M HNO_3 and 0.5 M H_2O_2 solution, followed by measurement of the soluble Mo species concentration in ICP-OES (Agilent 720, Agilent Technologies, Santa Clara, CA). Dispersions of chemically exfoliated MoS_2 samples were stored in 4 °C for further use. To prepare layer-stacked MoS_2 membranes, a dispersion containing 4 mg MoS_2 was filtered through a polyethersulfone (PES) ultrafiltration membrane with a nominal pore size of 30 nm (Sterlitech, Kent, WA), generating an MoS_2 membrane with a thickness of ~ 600 nm.

Metal ion adsorption by suspended MoS_2 nanosheets. Metal cation adsorption by MoS_2 nanosheets was studied in batch experiments. The metal cations tested include Mg^{2+}, K^{+}, Ca^{2+}, Ni^{2+}, Cd^{2+}, Zn^{2+}, Cu^{2+} and Pb^{2+} in their nitrate salt forms. After mixing MoS_2 nanosheets (100 mg/L) with individual cations (~ 5 mg/L) in 10 mL buffer solutions (MES, 10 mM, pH 6) for 1 d, cation-adsorbed nanosheets were removed through 0.22 μm PES syringe filters (VWR), and the cation concentrations in the filtrate solutions were determined using ICP-OES or ICP-MS (Agilent 7700 Series) for low concentration (≤ 10 μg/L). The removal is calculated as $R = 100 \times$

112 $(C_0 - C_f)/ C_0$ %, where C_0 and C_f are the initial and final cation concentrations (mg/L),
113 respectively. The distribution coefficient is calculated as $K_d = (V[(C_0 - C_f)/C_f])/m$, where V is the
114 solution volume (mL), and m is the adsorbent mass (g).

115 To characterize the competitive adsorption of metal cations, batch experiments were
116 carried out with a mixed solution containing ~5 mg/L of each cation (Mg^{2+}, K^+, Ca^{2+}, Ni^{2+}, Cd^{2+},
117 Zn^{2+}, Cu^{2+} and Pb^{2+}) and 100 mg/L MoS_2 nanosheets. A solution mimicking tap water
118 composition was prepared by spiking DI water with NaCl (280 mg/L), $CaCl_2$ (150 mg/L) and
119 $MgSO_4$ (75 mg/L). Batch tests were also used to understand the Pb^{2+} removal capacity, kinetics,
120 and selectivity.

121 In order to test the regeneration capability of MoS_2, we used a strong chelating agent
122 EDTA, which has a Pb-$EDTA^{2-}$ formation constant of approximately 10^{18} to recover Pb from
123 MoS_2. In each repeated test, 50 mg/L Pb^{2+} and 100 mg/L MoS_2 was added to 40 mL of pH 6
124 buffer solution, and the sample was then mixed for 2 h before the solid Pb-MoS_2 was collected by
125 vacuum-filtration onto a PES membrane. To recover the MoS_2, 40 mL of 5 mM EDTA solution
126 was added to the collected Pb-MoS_2 to allow the release of Pb from MoS_2 for 2 h, then the
127 regenerated MoS_2 was recollected by vacuum filtration for use in the next cycle.

128 **Pb removal by layer-stacked MoS_2 membranes.** The filtration experiments were performed
129 using a dead-end stirred cell filtration system (Model 8050, EMD Millipore) with a total internal
130 volume of 50 mL and an active surface area of 13 cm^2. The solution in the chamber was
131 continuously mixed with a suspended magnetic stirrer at 200 rpm. The chamber was filled with
132 aqueous solution containing Pb^{2+} at various concentrations (0.25, 1, 3 mg/L), which was
133 continuously supplied from a stock solution in a plastic container. The filtration experiments

were started by applying ~ 10 psi pressure to the chamber by means of compressed N_2. Ten-mL samples of the filtrate were periodically collected and analyzed by ICP-MS.

Density functional theory (DFT) simulations. All simulation results were calculated using DFT software VASP.[28] The exchange-correlation functional was described using generalized gradient approximation (GGA) with Perdew-Burke-Ernzerhof (PBE),[29] and the ion-electron interaction was treated with the projector augmented wave (PAW) method.[30] The cutoff energy was 520 eV and the energy convergence criterion was 10^{-5} eV/cell. The conjugate gradient method was adopted for the geometry optimization. The Brillouin zone was represented by a Monkhorst–Pack special k-point mesh[31] of different sizes depending on the MoS_2 size. For all calculations, the van der Waals (vdW) interaction was included using a dispersion correction term from the DFT-D3 method.[32] A large vacuum space of 30 Å was used to avoid any interaction of the MoS_2 sheets with their images. The electron localization function (ELF) calculation was also performed for detailed data analysis.[33] ELF is derived from the calculation of Pauli repulsion with values normalized between 0 and 1.[34] Notably, the Hubbard U correction was not added here since little changes were found for the electronic structure of MoS_2 in previous studies.[35-38]

Material and membrane characterization. MoS_2 nanosheets were characterized through transmission electron microscopy (TEM), atomic force microscopy (AFM), and X-ray photoelectron spectroscopy (XPS). TEM images were obtained with a JEM-2100F. The AFM images were obtained in air using a Bruker Dimension Icon in tapping mode. The XPS measurement was conducted with a K-Alpha XPS spectrometer (Thermo Scientific Ltd, East Grinstead, UK). The zeta potential measurement was performed on a Zetasizer Nano-ZSP analyzer (Malvern, Westborough, MA). Cross-sectional images of a layer-stacked MoS_2 were

recorded by a field emission SEM (Zeiss Gemini Ultra-55, Jena, Germany).

RESULTS AND DISCUSSION

Synthesis of MoS_2 nanosheets and layer-stacked membranes. We prepared MoS_2 monolayer nanosheets from MoS_2 bulk material through chemical exfoliation,[27, 39] engineered them into layer-stacked membranes, and tested the Pb removal by both configurations of MoS_2 (Figure 1a-c). The as-prepared MoS_2 nanosheets were highly dispersible in water because of their uniformly distributed negative charge on the surface (*e.g.*, each MoS_2 unit cell is believed to carry -0.25 eV),[40] as confirmed by a zeta potential of -40 to -50 mV in a wide pH range (Figure S1a). According to the TEM (Figure S1b) and AFM (Figure 1d) images, a majority of the exfoliated MoS_2 nanosheets had a lateral dimension of 100 to 500 nm and a monolayer thickness of ~1.1 nm. The phase composition of MoS_2 nanosheets characterized by XPS (Figure S1c-d) consisted of 40% 2H-MoS_2 and 60% 1T-MoS_2, which is consistent with the results of exfoliation-induced phase transformation reported previously.[39] Layer-stacked MoS_2 membranes were fabricated by filtration leading to a stable interlayer spacing of ~ 1.2 nm, which was naturally formed and stabilized by a balance between attractive van der Waals and repulsive hydration forces according to our previous study.[41] In this stacked configuration, MoS_2 membranes maintain an ultrahigh surface area, exposing all sulfur atoms on each nanosheet as accessible metal-binding sites, and thus potentially enabling a POU device with continuous water flow as well as high metal adsorption capacity.

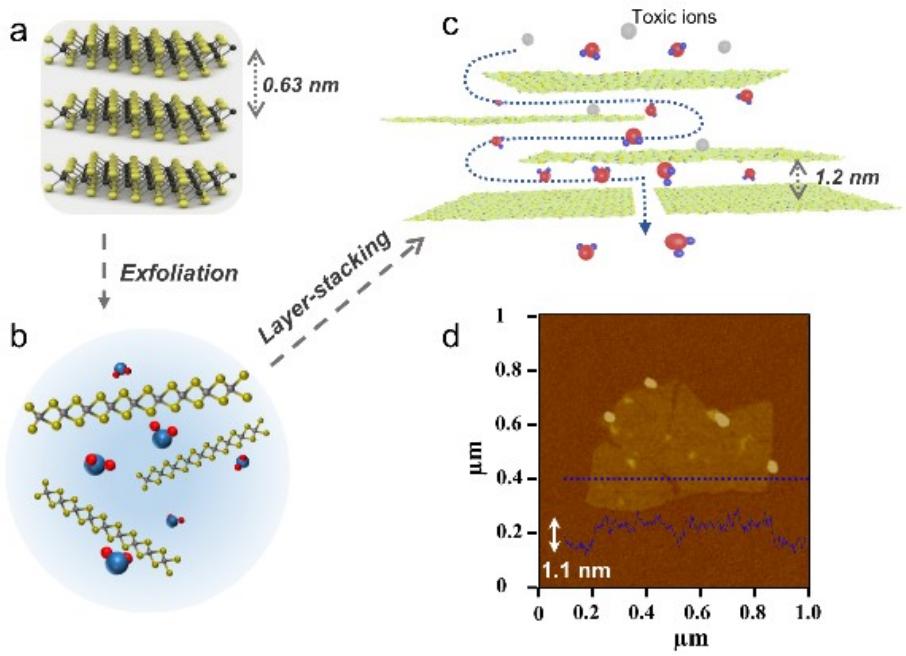

Figure 1. Schematic illustration of exfoliating bulk MoS_2 materials (a) to create an aqueous suspension of MoS_2 monolayer nanosheets (b) and reassembling the nanosheets into a layer-stacked MoS_2 membrane (c) for adsorptive filtration targeting the removal of toxic ions. (d) The AFM image of a monolayer MoS_2 nanosheet with a depth profile revealing a thickness of ~ 1.1 nm.

Selectivity of MoS_2 nanosheets towards different cations. To determine the selectivity of MoS_2 towards different cations, we first evaluated the adsorption of several toxic transition metal cations (Ni^{2+}, Cd^{2+}, Zn^{2+}, Cu^{2+} and Pb^{2+}) and some common background cations (Mg^{2+}, K^{+}, Ca^{2+}) by MoS_2 monolayers in batch experiments (see details in Table S1 and S2). Figure 2a (blue hatched bars) shows the calculated removal of various cations in individual ion tests. MoS_2 nanosheets demonstrated nearly complete removal of Pb^{2+} and Cu^{2+} by effectively decreasing their concentrations from 5 mg/L, to 4 and 1 μg/L respectively. In comparison, the removal efficiency was relatively high (~ 90%) for Cd^{2+}, moderate (30 to 50%) for Zn^{2+}, Ni^{2+} and Ca^{2+}, and very low (< 20%) for Mg^{2+} and K^{+}. In addition, the high affinity of MoS_2 nanosheets towards Pb^{2+} can be demonstrated by a low threshold concentration (0.1 mM) that induces visible aggregation of

MoS_2 nanosheets within half an hour. While for poorly adsorbed ions (e.g., Mg^{2+}), a higher threshold concentration for aggregation (0.5 mM) was observed (Figure S2).[42]

To directly compare the affinity of MoS_2 nanosheets towards different cations in a competitive environment, we also conducted the adsorption experiments in an ion mixture containing all eight cations of the same concentration (~ 5 mg/L). As shown in Figure 2a (red unhatched bars), MoS_2 nanosheets maintained excellent removal of Pb^{2+} and Cu^{2+} by decreasing their concentrations from ~ 5 mg/L to a few micrograms per liter, which was in good agreement with those observed in individual ion tests. However, the removal of each of the other cation species was much lower than that when tested individually, indicating that the preferred adsorption of Cu^{2+} and Pb^{2+} significantly decreased the available sorption sites for other ions.

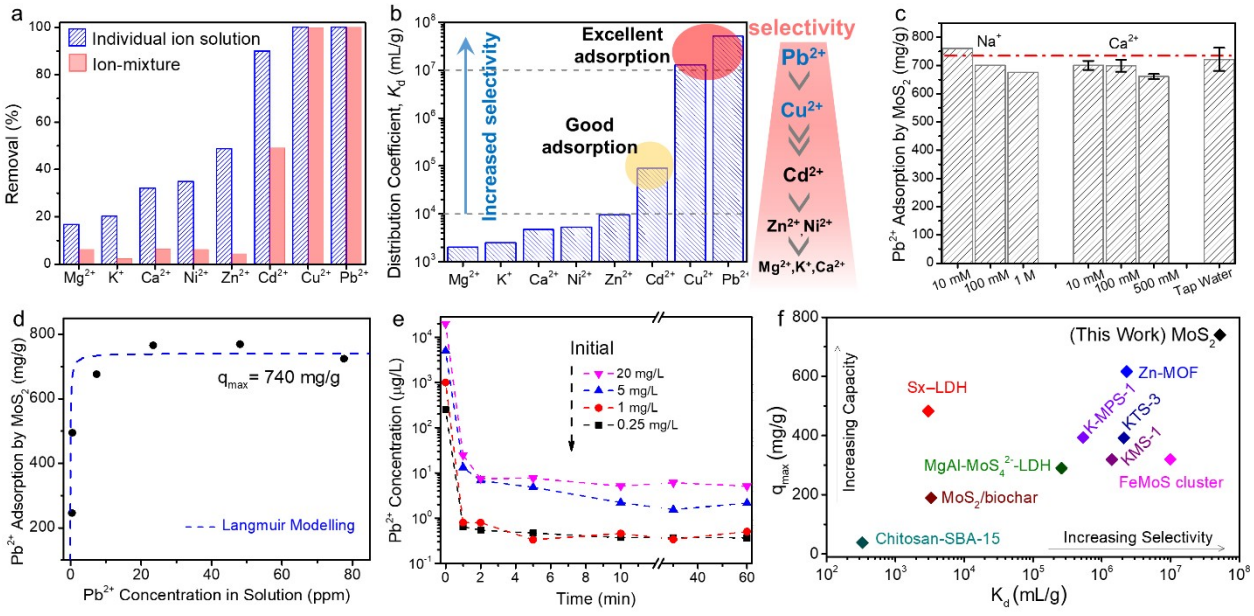

Figure 2. Characterization of the selectivity and capacity of Pb^{2+} adsorption by suspended MoS_2 nanosheets. (a) Removal of various cations by MoS_2 nanosheets in individual ion solutions and in a mixture containing all ions of equal concentration (5 mg/L). (b) Distribution coefficients K_d of various cation species. (c) Pb^{2+} removal by MoS_2 in the presence of Na^+, Ca^{2+} or tap water impurities. The dashed line represents the maximum removal capacity observed in the pure water baseline experiment. (d) Isotherm of Pb^{2+} adsorption by MoS_2 fitted by Langmuir model (dash line). (e) Kinetics of Pb^{2+} adsorption

at various initial Pb^{2+} concentrations. (f) Comparison of the adsorption capacity (q_{max}) and distribution coefficient (K_d) of MoS_2 nanosheets with those of other benchmark materials reported in the literature.[6, 11, 43-55]

The affinity of MoS_2 nanosheets to various cations can be compared by calculating their distribution coefficients K_d (Figure 2b). According to the individual cation test results, the K_d values of MoS_2 nanosheets for Pb^{2+} and Cu^{2+} are both $>10^7$ mL/g, which are 2 to 4 orders of magnitude higher than those for other metal cations, revealing the excellent adsorptive selectivity of MoS_2 nanosheets towards Pb^{2+} and Cu^{2+}. To further reveal the relative affinity of MoS_2 nanosheets to Pb^{2+} and Cu^{2+}, we conducted competitive tests where the initial concentrations of Cu^{2+} and Pb^{2+} remained constant at ~ 5 mg/L, but the initial concentrations of MoS_2 nanosheets were reduced from 100 mg/L to 30, 15, and 5 mg/L, respectively. As shown in Figure S3 and Table S3, at lower concentrations (30 and 15 mg/L) of MoS_2 nanosheets, Pb^{2+} removal was still close to 100%, while the removal of Cu^{2+} decreased from 100% to 91.2% and 36.1% respectively. These results indicate that when MoS_2 was limited in quantity, its adsorption sites highly preferred Pb^{2+} over Cu^{2+}. Only when the concentration of MoS_2 further decreased to 5 mg/L was there a slight decline in Pb^{2+} removal, whereas Cu^{2+} removal was very low (6.1%).

Overall, the MoS_2 monolayer displayed an adsorption affinity in the order $Pb^{2+} > Cu^{2+} >> Cd^{2+} > Zn^{2+}$, $Ni^{2+} > Mg^{2+}$, K^+, Ca^{2+} (Figure 2b). This is consistent with the hard-soft principle in Lewis acid-base theory, i.e., the sulfur sites on MoS_2 offer strong soft-soft interactions towards soft acids (metal ions such as Pb^{2+}, Cu^{2+}, and Cd^{2+}). The high affinity/selectivity towards Pb^{2+} over hard acid species (Mg^{2+}, K^+, Ca^{2+}) reveals the great promise of using MoS_2 nanosheets in the development of household POU devices for the removal of lead from drinking water. In addition, we tested the interference of Pb^{2+} adsorption by high concentrations of common cations (e.g., Na^+

234 and Ca^{2+}) that are ubiquitous in drinking water. We found that the presence of a high
235 concentration of these background ions (up to 1 M $NaNO_3$, 1 M $Ca(NO_3)_2$, or concentrations
236 characteristic of a tap water mimic, with detailed composition data in the Supporting
237 Information) did not affect Pb^{2+} removal by MoS_2 (Figure 2c).

238 The Pb^{2+} adsorption capacity and kinetics were further studied to elucidate the removal
239 mechanism. The adsorption of Pb^{2+} onto MoS_2 monolayers was examined by varying the initial
240 Pb^{2+} concentration in the range of 25 to 150 mg/L. As shown in Figure 2d, the adsorption
241 isotherm data can be better fitted by the Langmuir model than the Freundlich model (Figure S4),
242 indicating the adsorption of a monolayer Pb^{2+} onto the MoS_2 nanosheet surface. According to the
243 model, MoS_2 nanosheets have a maximum adsorption capacity of 740 mg/g toward Pb^{2+} (Figure
244 2d and Figure S5). The Pb^{2+} removal also depends on pH conditions (Figure S6). Higher removal
245 capacity is found at neutral pH (~ 740 mg/g) than at acidic conditions (e.g., ~ 350 mg/g at pH 3).
246 The decrease in Pb^{2+} adsorption at lower pH indicates that the Pb^{2+} captured by MoS_2 may be
247 attributed to the ion exchange with protons on the nanosheets ($H_{0.25}MoS_2$),[40] the deprotonation of
248 which is inhibited by low pH. Similar Pb^{2+} adsorption mechanisms and pH effects have been
249 observed with other functional materials.[43, 55] In this study, pH 6 was adopted to investigate the
250 fundamental interactions between MoS_2 and Pb^{2+} in order to avoid the interference of possible
251 hydroxide precipitate at alkaline conditions. Fast removal kinetics (2-3 logs Pb^{2+} removal within 2
252 min, as shown in Figure 2e) was observed regardless of initial Pb^{2+} concentration in solution
253 (0.25 to 20 mg/L). The regeneration of MoS_2 can be achieved by using strong chelating agents
254 with a formation constant higher than $10^{11.4}$ (Figure S7). In our study, EDTA with a formation
255 constant of 10^{18} was chosen for regeneration. The regeneration of MoS_2 could maintain a 85-95%
256 lead removal in 2 to 5 repeated regeneration cycles (Figure S8). The slight reduction in removal

efficiency during regeneration was likely caused by the aggregation or partial oxidation of MoS_2 nanosheets.

Overall, the MoS_2 nanosheets studied in this work have superior lead adsorption capabilities compared with other materials reported so far. As shown in Figure 2f, our exfoliated MoS_2 nanosheets demonstrate a high Pb^{2+} adsorption capacity (740 mg/g) and an extremely high affinity K_d ($5.2\pm1.9\times10^7$ mL/g), outperforming previously reported materials including MOFs, layered metal sulfides, and sulfur-functionalized nanomaterials.[6, 11, 43-49] Note that adsorbents with K_d values in the order of magnitude of 10^4 are considered to have outstanding selectivity.[56] Examples include sulfur-based sorbents such as S_x- and MoS_4^{2-}-intercalated LDH (10^3 to 2.6×10^5 mL/g),[11, 46] layered metal sulfides (5.4×10^5 to 2.1×10^6 mL/g),[43, 47, 49] MoS_2 hydrogel (1.32×10^4 mL/g),[50] and others (10^3-10^5 mL/g).[53-55] More details can be found in Table S4. The MoS_2 nanosheets indeed exhibit the highest K_d (10^7 mL/g) among all materials to the best of our knowledge, demonstrating their excellent selectivity toward Pb^{2+}.

Investigation of adsorption mechanism. To further elucidate the adsorption mechanisms, we used DFT simulation based on first-principle calculations to study the interactions between metal ions and 2H-MoS_2. 2H-MoS_2 was chosen for modelling because of its thermodynamic stability and common presence in nature. As MoS_2 nanosheets are partially reduced during the intercalation/exfoliation process, they are negatively charged and have a formula of $H_{0.25}MoS_2$ or $MoS_2^{-0.25}$.[40] According to this formula, we built a 4×4 MoS_2 supercell with 4 hydrogen atoms evenly distributed on the surface ($H_4(MoS_2)_{16}$, Figure S14). Since all reactions take place in aqueous solution, the ions are present in the hydrated form, and the number of water molecules in the hydration shell is determined based on literature data.[57] Therefore, the adsorption of a divalent

279 metal ion (M^{2+}) onto MoS_2 can be described in equation 1.

280 $H_4(MoS_2)_{16} + n$¿ (1)

281 where *n* varies in the range of 1 to 24 depending on the Pb/S coverage ratio ranging from 1/32 to

282 3/4. Accordingly, the corresponding free energy of adsorption ($\Delta G_{f,ads}$) is calculated by the

283 following equation:

284 $\Delta G_{f,ads} = E_{[M_n(MoS_2)_{16}]^{2n-4}} + 4E_{(H_2O)_2H^+}$¿ $+ (n-2)E_{(H_2O)_4} - E_{H_4(MoS_2)_{16}} - nE_{(H_2O)_4M^{2+}}$¿ (2)

285 where *E* represents the internal energy of the corresponding compound, which can be obtained

286 from the first-principle DFT calculations. A detailed illustration of the adsorption reaction and

287 the methodology used to calculate the free energy is discussed in the Supporting Information. A

288 negative free energy $\Delta G_{f,ads}$ indicates that the adsorption is energetically favorable, and vice versa.

289

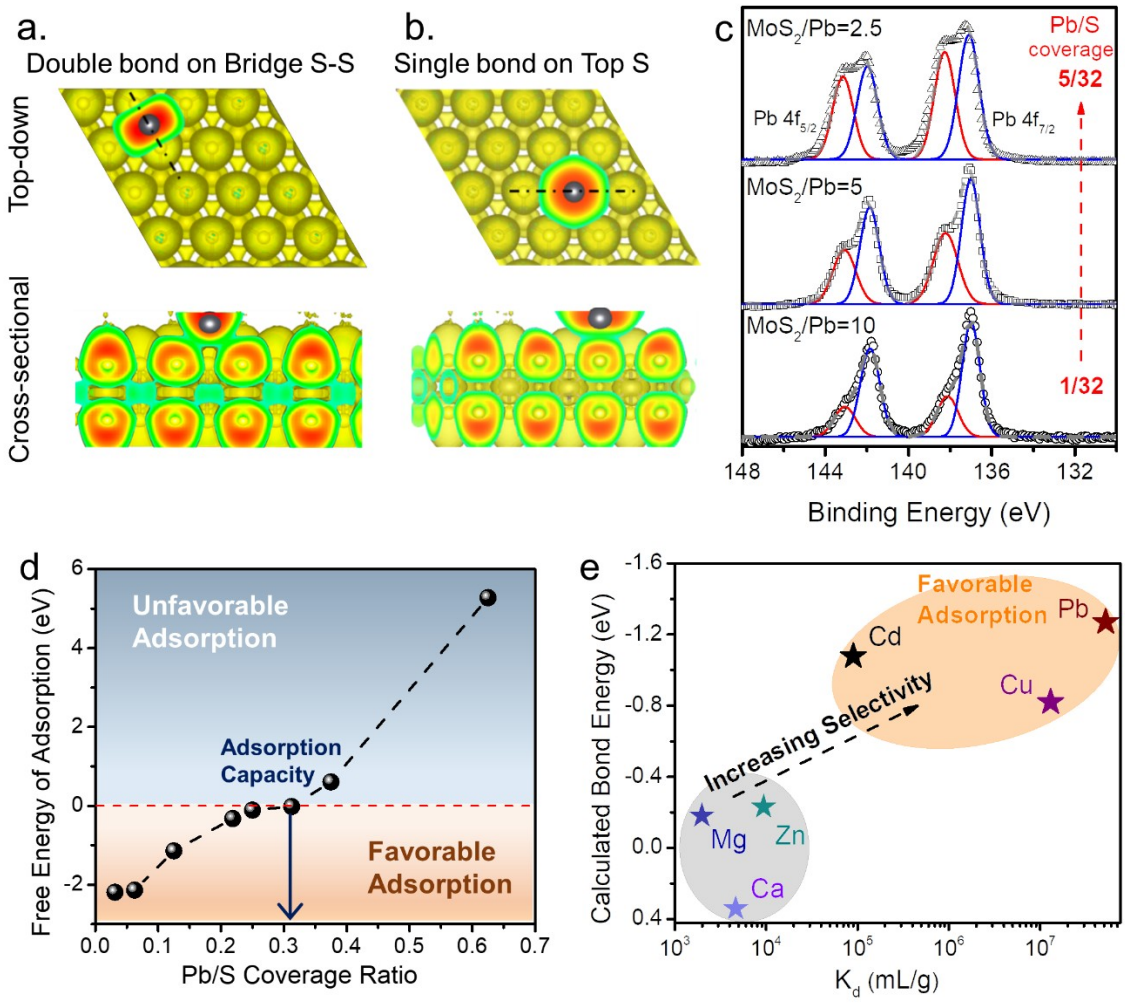

Figure 3. Mechanistic investigation of lead adsorption by DFT simulation and XPS spectra. The top-down and cross-sectional views of the electron localization function (ELF, with detailed explanation in Supporting Information) for the Pb-MoS_2 double bond formed on a bridge S-S site (a) and a single bond formed on a top-S site (b). (c) XPS spectra of Pb peaks with the Pb/S coverage ratio increasing from 1/32 to 5/32, which correspond to the MoS_2-Pb mass ratio ranging from 10 to 2.5 (see SI for calculation process). The peaks at higher (red) and lower (blue) binding energies are most likely attributed to single bonds on the top-S and double bonds on the bridge S-S sites, respectively. (d) The free energy of Pb^{2+} adsorption on MoS_2 surface as a function of Pb/S coverage ratio. (e) The maximum bond energy for the binding between cations and MoS_2.

The binding mechanisms between Pb^{2+} and MoS_2 nanosheets are affected by the Pb/S coverage ratio. The most stable (energetically favorable) binding site on MoS_2 is the Bridge S-S site (Figure 3a), where a Pb^{2+} binds to two neighboring S-atoms with an equal bond length of ~ 2.7 Å. However, when the Pb/S coverage ratio increases, the dominating binding site shifts to the

304 Top-S site, where a Pb^{2+} binds to only one S atom with a bond length of ~ 2.5 Å (Figure 3b). The
305 Pb-MoS_2 double bond formed at the Bridge S-S position (binding energy of -1.3 eV) is stronger
306 than the single bond at the Top-S position (binding energy of -1.0 eV). A more detailed
307 description of the binding mechanism, formation energy, bond length, geometry, and effects of
308 Pb-S coverage can be found in Tables S5 and S6, Figures S19 to S22. The simulation results are
309 correlated with the deconvolution of Pb 4f peaks in the XPS spectra at different Pb/S coverage
310 ratios. As shown in Figure 3c, when the Pb/S coverage ratio increases from 1/32 to 5/32 (i.e., the
311 MoS_2/Pb mass ratio decreases from 10 to 2.5), the component peak at higher binding energy (red
312 line) increases in strength, corresponding to more single bonds on Top-S sites, while the
313 component peak at lower binding energy (blue line) becomes weaker, corresponding to less
314 double bonds on the Bridge-S-S sites. The XPS results are consistent with the simulation results.
315 The overall free energy ($\Delta G_{f,ads}$) for Pb adsorption onto MoS_2 is strongly affected by the
316 Pb/S coverage (Figure 3d). The free energy of adsorption increases with increasing Pb/S coverage
317 ratio, indicating that the adsorption of Pb becomes weaker when more Pb is adsorbed onto MoS_2
318 surfaces. The free energy becomes positive when Pb/S coverage is over 0.31, demonstrating that
319 the adsorption of more Pb beyond the 31% coverage is energetically unfavorable. The 31%
320 coverage amounts to an adsorption capacity of 802 mg/g, which is very close to our experimental
321 results (740 mg/g).
322 To understand the stronger selectivity towards Pb^{2+} than towards other cations, the binding
323 energy for other cations were also calculated using the DFT model. The favorable binding
324 mechanism for each metal species is shown in Table S7. It was found that for almost all divalent
325 cations except Ca^{2+}, the most stable (energetically favorable) binding mechanism is the double

bond formed at Bridge S-S sites. The binding of Ca^{2+} is unique because the bonds on all binding sites exhibit a positive formation energy, indicating unfavorable adsorption. The formation energy of the most favorable binding of each cation on the MoS_2 nanosheet is correlated with the experimentally measured K_d values in Figure 3e. In general, a negative formation energy of around -1 eV (for Pb^{2+}, Cd^{2+}, and Cu^{2+}) corresponds to a high K_d value (above 10^5 mL/g), demonstrating good consistency between simulation and experimental results. Among all metal ions analyzed, the formation energy of Pb-MoS_2 has the most negative value (-1.3 eV), indicating stronger bonding and more facile interactions of Pb^{2+} than those of Cu^{2+} and Cd^{2+} with MoS_2 nanosheets, consistent with its highest K_d value measured experimentally. The formation energy of Zn^{2+}, Mg^{2+} and Ca^{2+} is much less negative or becomes positive (> - 0.4 eV), consistent with their low K_d values (below 10^4 mL/g) measured experimentally. It's worth noting that the interactions between MoS_2 and representative ions were simulated exclusively with 2H-MoS_2, and the potential effects of various MoS_2 phases on the adsorption efficiency should be investigated via experimental tests and theoretical simulations in the future studies.

Besides adsorption, metal ion removals can be potentially caused by redox reactions and/or precipitation formation with MoS_2 nanosheets or soluble molybdate species. To explore if these mechanisms are present in removing Pb^{2+} and other metal ions tested here, we carried out extensive XPS characterization of the metal-adsorbed MoS_2 samples (Pb-, Cu-, Cd-, Ni-, Zn-MoS_2). As shown in Figure S9a, compared to the pristine MoS_2, all metal-adsorbed MoS_2 samples exhibit similar Mo and S peak positions and intensities. Meanwhile, the absence of oxidized S at 168 eV and constant 1T/2H ratios indicate no direct redox reaction occurring between MoS_2 and metal species tested here (Figure S9b and S9c). This is consistent with the previous findings that MoS_2 can not reduce Pb^{2+}or Cu^{2+}, although redox reaction contributes

greatly to the removal of Ag^{+} and Hg^{2+} that leads to oxidized S and reduced 1T/2H ratios.[26] We observed weak peaks of molybdate, which often co-exists in the MoS_2 suspension due to slow oxidative dissolution of MoS_2 by ambient oxygen. Based on the XPS characterization (Figure S9b), even if we assume all the molybdate contributes to Pb removal by forming precipitates, the precipitation accounts for less than ~10 % of the total Pb removal (see Supporting Information for calculation).

Layer-stacked MoS_2 as POU filter. Excellent capacity and selectivity are the pre-requisites for MoS_2 monolayers as potential building blocks for a POU filter. With these aspects demonstrated above, we further used MoS_2 monolayers to synthesize a layer-stacked MoS_2 membrane, and explored its potential for POU removal of lead from drinking water. The MoS_2 membranes were tested in filtration experiments with feed water containing various concentrations of Pb^{2+}. The membrane maintained a constant water flux (145 L m^{-2} h^{-1} bar^{-1}) due to stable 2D nanochannels formed between stacked MoS_2 nanosheets with an interlayer distance of 1.2 nm (Figure S10). The interlayer spacing is large enough to allow Pb^{2+} to enter the 2D nanochannels in the MoS_2 membrane and adsorb it onto the channel walls. As a result, Pb^{2+} concentration is efficiently lowered from 0.25-3 mg/L in the feed water, to less than 10 µg/L in the effluent, which is the WHO guideline value. Since the MoS_2 membrane mainly removes Pb^{2+} by adsorption, there would be a breakthrough point when the effluent concentration rises above 10 µg/L. The total effluent volume at the breakthrough point defines the treatment capacity of the adsorptive membrane. As shown in Figure 4a, when the Pb^{2+} concentration in feed water was 0.25, 1, and 3 mg/L, the treatment capacity of the MoS_2 membrane was 800, 180, and 70 mL, respectively. It is

estimated that the residence time of Pb^{2+} in the MoS_2 membrane is merely 0.02 s (see calculation in Figure S10), so the breakthrough is most likely controlled by a dynamic process instead of reaching an equilibrium condition for adsorption. Therefore, the treatment capacity of MoS_2 membranes can be further improved by increasing the residence time, e.g., by synthesizing a thicker membrane (Figure S12).

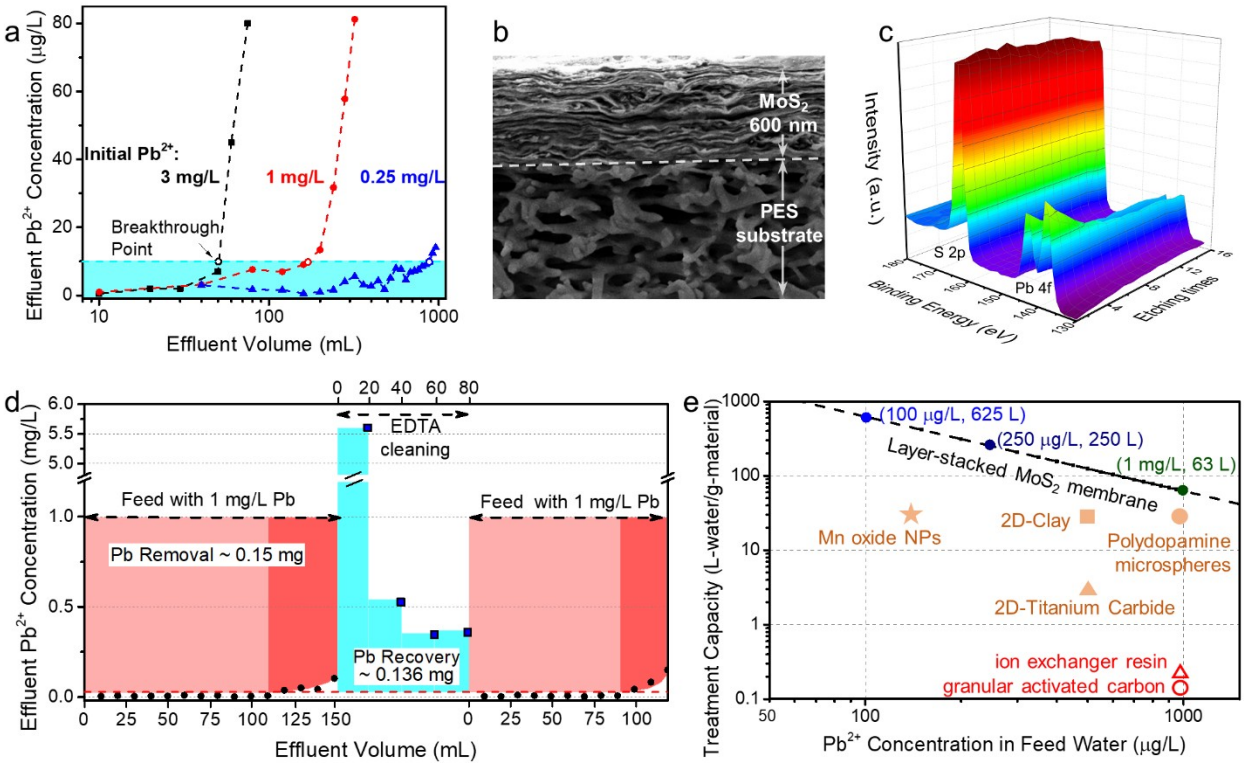

Figure 4. Layer-stacked MoS_2 membrane as a POU filter. (a) The performance of MoS_2 membranes in filtering a feed water containing 0.25 to 3 mg/L Pb^{2+}. The treatment capacity is defined as the total effluent volume at the breakthrough point, which was reached when the effluent Pb^{2+} concentration reached 10 μg/L. The cross-sectional SEM (b) and XPS depth profile (c) of the MoS_2 membrane after filtering Pb^{2+} water (see Figure S11 for detailed peak intensity evolution). (d) The regeneration of MoS_2 membrane using EDTA cleaning. (e) Treatment capacities (L-water/g-material) of MoS_2 membranes and other adsorptive membranes reported in the literature. Membranes fabricated by commercial materials are represented by red hollow symbols, and those by lab-synthetic materials are represented by amber filled symbols.

SEM and XPS were used to characterize a used MoS_2 membrane after being tested with 1 mg/L Pb^{2+} feed solution and reaching the breakthrough point in filtration. The MoS_2 membrane

maintains a stacked structure as shown in the cross-sectional SEM image (Figure 4b). The distribution of adsorbed lead in the MoS_2 membrane can be observed in the depth profile of the S 2p and Pb 4f peaks obtained by etching 300 nm (15 times × 20 nm etching depth) into the MoS_2 membrane during XPS characterization (Figure 4c). The Pb/S atomic ratio is high (12 %) on the membrane surface, and gradually decreases to around 5 % at 100 nm depth and below. The higher Pb content on the membrane top surface could be partially attributed to the diffusion of Pb^{2+} ions from water during drying. The relatively constant Pb/S ratio in the membrane interior confirms that adsorption instead of membrane exclusion is the dominant Pb^{2+} removal mechanism.

The regeneration ability of the MoS_2 membrane was evaluated by using EDTA cleaning to remove the adsorbed Pb^{2+} ions from the membrane after a filtration experiment. As shown in Figure 4d, the MoS_2 membrane adsorbed 0.15 mg Pb^{2+} from the first filtration cycle, and the EDTA cleaning by flushing with 80 mL EDTA solution recovered approximately 0.136 mg Pb^{2+} from the membrane, leading to a recovery of more than 90 %. It is worth noting that the concentration of recovered Pb^{2+} in the first 20 mL EDTA solution was as high as 5.5 mg/L, demonstrating the effectiveness in regenerating MoS_2 membranes. A second filtration cycle was performed after EDTA cleaning, and the regenerated MoS_2 membrane could reduce Pb^{2+} concentration to less than 10 µg/L with a treatment capacity of 90 mL, equivalent to nearly 90% of the original treatment capacity of a fresh MoS_2 membrane.

The treatment capacity of a POU filter is calculated by considering a conservative 65.6 mg/g lead removal capacity of the MoS_2 membrane (based on the tests shown in Figure S12). As shown in Figure 4e, the POU device demonstrates a treatment capacity of 63 to 625 L-water/g-MoS_2 depending on the initial Pb^{2+} concentration in tap water. For instance, when Pb^{2+}

411 concentration in the water is 100 and 250 μg/L, a POU device containing 1 g of MoS_2 membrane
412 could effectively treat 625 and 170 L water, respectively. The treatment capacity of MoS_2
413 membrane is several orders of magnitude higher than that of adsorptive membranes made of
414 commercial or lab-synthetic materials reported in the literature [12, 58, 59]. The superb performance
415 can be attributed to the high adsorption capacity and selectivity of MoS_2 nanosheets as well as
416 the fully accessible sulfur sites in the 1.2-nm 2D nanochannels enabled by the layer-stacking
417 structure.

418 The leaching of MoS_2 nanosheets and soluble Mo species from MoS_2 membranes is also
419 characterized in the filtration experiments. During the Pb adsorption and EDTA cleaning process,
420 we observed a low concentration of leached Mo species (< 0.1 mg/L) in the filtrate (Figure S13).
421 This is due to the slow oxidation of chemically exfoliated MoS_2 to soluble molybdate ions as was
422 reported previously.[60] To the best of our knowledge, molybdate ions have not been reported to
423 generate environmental toxicity or negative human health impacts at such low concentrations.
424 The leaching problem can also be potentially addressed by using more stable MoS_2 prepared by
425 ultrasonication, which significantly slows down Mo leaching (Figure S13). Loose nanosheets
426 were not observed throughout all filtration tests, nor during a batch test where external pressure
427 was removed, a condition that can accelerate nanosheet release if applicable (Figure S14). This
428 structural stability is consistent with our previous finding that the strong vdW forces between
429 MoS_2 nanosheets could potentially prevent the layer-stacked MoS_2 nanosheets from releasing in
430 water.[41]

431 **Environmental Implications.** Our findings suggest that emerging 2D MoS_2 nanosheets can find
432 important applications like lead removal from drinking water. MoS_2's superb lead adsorption

capabilities are evidenced by its adsorption capacity (740 mg/g) and its extremely high distribution coefficient K_d (5.2×10^7 mL/g), both of which are among the highest for materials that have ever been reported to the best of our knowledge. Additionally, once assembled into a layer-stacked membrane, the unique 1.2-nm 2D nanochannels formed between MoS_2 nanosheets make all the surface sulfur sites fully accessible for lead adsorption, while allowing water to permeate through the membrane at a fast speed. The layer-stacked MoS_2 membrane could effectively remove Pb^{2+} in drinking water from a few mg/L to less than 10 μg/L, with a treatment capacity a few orders of magnitude higher than that of membrane filters fabricated with commercial or other nanomaterials. An additional advantage of the MoS_2 membrane is that the nanochannels also enable the rejection of lead-containing particulates, a common form of lead contamination in tap water due to the corrosion of drinking water distribution pipes.[61] MoS_2 has also been reported to have excellent antimicrobial/antifouling properties,[62, 63] another important feature for multi-functional membrane applications. With exfoliation and synthesis methodology maturing, the cost and complexity of MoS_2 nanosheet production is expected to continuously decrease. Therefore, we believe that MoS_2 membrane-based technology holds great promise as a POU device installed in households, schools, or public utilities to remediate lead contamination and safeguard drinking water quality for the public.

Associated Content

Supporting Information

The Supporting Information is available free of charge on the ACS Publications website. This document includes additional characterization of MoS_2 nanosheets and membranes, supplementary adsorption results, DFT modeling process and results.

Acknowledgements

The material is based upon work supported by U.S. National Science Foundation (NSF) under award nos. CBET-1565452 and CBET-1706059. Work at the Molecular Foundry was supported by the Office of Science, Office of Basic Energy Sciences, of the U.S. Department of Energy under contract no. DE-AC02-05CH11231. Work at SUSTech was supported by SUSTech-MIT Joint Center for Mechanical Engineering Education and Research, and State Environmental Protection Key Laboratory of Integrated Surface Water-Groundwater Pollution Control. The authors acknowledge the assistance of SUSTech Core Research Facilities. The opinions expressed herein, however, are those of the authors and do not necessarily reflect those of the sponsors. Z Wang and Q Tu contributed equally to this work.

References

1. Pieper, K. J.; Tang, M.; Edwards, M. A., Flint water crisis caused by interrupted corrosion control: Investigating "ground zero" home. *Environ. Sci. Technol.* **2017,** *51*, (4), 2007-2014.
2. Pieper, K. J.; Nystrom, V. E.; Parks, J.; Jennings, K.; Faircloth, H.; Morgan, J. B.; Bruckner, J.; Edwards, M. A., Elevated lead in water of private wells poses health risks: case study in Macon County, North Carolina. *Environ. Sci. Technol.* **2018,** *52*, (7), 4350-4357.
3. US-EPA, Maximum contaminant level goals and national primary drinking water regulations for lead and copper; final rule. In Federal Register: 1991.
4. WHO, Guidelines for drinking-water quality In World Health Organization: 1993.
5. Ngueta, G.; Abdous, B.; Tardif, R.; St-Laurent, J.; Levallois, P., Use of a cumulative exposure index to estimate the impact of tap water lead concentration on blood lead levels in 1-to 5-year-old children (Montréal, Canada). *Environ. Health Perspect.* **2016,** *124*, (3), 388.
6. Yu, C.; Shao, Z.; Hou, H., A functionalized metal–organic framework decorated with O– groups showing excellent performance for lead (II) removal from aqueous solution. *Chem. Sci.* **2017,** *8*, (11), 7611-7619.
7. Sun, D. T.; Peng, L.; Reeder, W. S.; Moosavi, S. M.; Tiana, D.; Britt, D. K.; Oveisi, E.; Queen, W. L., Rapid, selective heavy metal removal from water by a metal–organic framework/polydopamine composite. *ACS Cent. Sci.* **2018,** *4*, (3), 349-356.
8. Zhao, G.; Li, J.; Ren, X.; Chen, C.; Wang, X., Few-layered graphene oxide nanosheets as

superior sorbents for heavy metal ion pollution management. *Environ. Sci. Technol.* **2011,** *45*, (24), 10454-10462.
9. Sun, Q.; Aguila, B.; Perman, J.; Earl, L. D.; Abney, C. W.; Cheng, Y.; Wei, H.; Nguyen, N.; Wojtas, L.; Ma, S., Postsynthetically modified covalent organic frameworks for efficient and effective mercury removal. *J. Am. Chem. Soc.* **2017,** *139*, (7), 2786-2793.
10. Huang, N.; Zhai, L.; Xu, H.; Jiang, D., Stable covalent organic frameworks for exceptional mercury removal from aqueous solutions. *J. Am. Chem. Soc.* **2017,** *139*, (6), 2428-2434.
11. Ma, L.; Wang, Q.; Islam, S. M.; Liu, Y.; Ma, S.; Kanatzidis, M. G., Highly selective and efficient removal of heavy metals by layered double hydroxide intercalated with the MoS_4^{2-} ion. *J. Am. Chem. Soc.* **2016,** *138*, (8), 2858-2866.
12. Peng, Q.; Guo, J.; Zhang, Q.; Xiang, J.; Liu, B.; Zhou, A.; Liu, R.; Tian, Y., Unique lead adsorption behavior of activated hydroxyl group in two-dimensional titanium carbide. *J. Am. Chem. Soc.* **2014,** *136*, (11), 4113-4116.
13. Li, Z.; Fan, R.; Hu, Z.; Li, W.; Zhou, H.; Kang, S.; Zhang, Y.; Zhang, H.; Wang, G., Ethanol introduced synthesis of ultrastable 1T-MoS_2 for removal of Cr(VI). *J. Hazard. Mater.* **2020,** *394*, 122525.
14. Chen, Z.; Zhang, S.; Liu, Y.; Alharbi, N. S.; Rabah, S. O.; Wang, S.; Wang, X., Synthesis and fabrication of g-C_3N_4-based materials and their application in elimination of pollutants. *Sci. Total Environ.* **2020**, 139054.
15. Hu, B.; Ai, Y.; Jin, J.; Hayat, T.; Alsaedi, A.; Zhuang, L.; Wang, X., Efficient elimination of organic and inorganic pollutants by biochar and biochar-based materials. *Biochar* **2020,** *2*, (1), 47-64.
16. Wang, Z.; Mi, B., Environmental applications of 2D molybdenum disulfide (MoS_2) nanosheets. *Environ. Sci. Technol.* **2017,** *51*, (15), 8229-8244.
17. Fausey, C. L.; Zucker, I.; Lee, D. E.; Shaulsky, E.; Zimmerman, J. B.; Elimelech, M., Tunable Molybdenum Disulfide-Enabled Fiber Mats for High-Efficiency Removal of Mercury from Water. *ACS Appl. Mater. Interfaces* **2020,** *12*, (16), 18446-18456.
18. Ai, K.; Ruan, C.; Shen, M.; Lu, L., MoS_2 nanosheets with widened interlayer spacing for high-efficiency removal of mercury in aquatic systems. *Adv. Funct. Mater.* **2016,** *26*, (30), 5542-5549.
19. Subrahmanyam, K. S.; Malliakas, C. D.; Sarma, D.; Armatas, G. S.; Wu, J.; Kanatzidis, M. G., Ion-exchangeable molybdenum sulfide porous chalcogel: Gas adsorption and capture of iodine and mercury. *J. Am. Chem. Soc.* **2015,** *137*, (43), 13943-13948.
20. Wang, J.; Zhang, W.; Yue, X.; Yang, Q.; Liu, F.; Wang, Y.; Zhang, D.; Li, Z.; Wang, J., One-pot synthesis of multifunctional magnetic ferrite–MoS_2–carbon dot nanohybrid adsorbent for efficient Pb(II) removal. *J. Mater. Chem. A* **2016,** *4*, (10), 3893-3900.
21. Zhao, H.; Yang, G.; Gao, X.; Pang, C. H.; Kingman, S. W.; Wu, T., Hg0 capture over CoMoS/γ-Al_2O_3 with MoS_2 nanosheets at low temperatures. *Environ. Sci. Technol.* **2016,** *50*, (2), 1056-1064.
22. Luo, J.; Fu, K.; Sun, M.; Yin, K.; Wang, D.; Liu, X.; Crittenden, J. C., Phase-mediated heavy metal adsorption from aqueous solutions using two-dimensional layered MoS_2. *ACS Appl. Mater. Interfaces* **2019,** *11*, (42), 38789-38797.
23. Zhang, L.; He, X.; Zhou, Q.; Hu, X., Fabrication of 1T-MoS_2 nanosheets and the high-

efficiency removal of toxic metals in aquatic systems: Performance and mechanisms. *Chem. Eng. J.* **2020,** *386*, 123996.
24. Kumar, N.; Fosso-Kankeu, E.; Ray, S. S., Achieving controllable MoS_2 nanostructures with increased interlayer spacing for efficient removal of Pb(II) from aquatic systems. *ACS Appl. Mater. Interfaces* **2019,** *11*, (21), 19141-19155.
25. Li, D. O.; Gilliam, M. S.; Debnath, A.; Chu, X. S.; Yousaf, A.; Green, A. A.; Wang, Q. H., Interaction of Pb^{2+} ions in water with two-dimensional molybdenum disulfide. *J. Phys. Mater* **2020,** *3*, (2), 024007.
26. Wang, Z.; Sim, A.; Urban, J. J.; Mi, B., Removal and recovery of heavy metal ions by two-dimensional MoS_2 nanosheets: performance and mechanisms. *Environ. Sci. Technol.* **2018,** *52*, (17), 9741-9748.
27. Joensen, P.; Crozier, E.; Alberding, N.; Frindt, R., A study of single-layer and restacked MoS_2 by X-ray diffraction and X-ray absorption spectroscopy. *J. Phys. C: Solid State Phys.* **1987,** *20*, (26), 4043.
28. Kresse, G.; Furthmüller, J., Efficient iterative schemes for ab initio total-energy calculations using a plane-wave basis set. *Phys. Rev. B* **1996,** *54*, (16), 11169.
29. Perdew, J. P.; Burke, K.; Ernzerhof, M., Generalized gradient approximation made simple. *Phys. Rev. Lett.* **1996,** *77*, (18), 3865.
30. Blöchl, P. E., Projector augmented-wave method. *Phys. Rev. B* **1994,** *50*, (24), 17953.
31. Monkhorst, H. J.; Pack, J. D., Special points for Brillouin-zone integrations. *Phys. Rev. B* **1976,** *13*, (12), 5188.
32. Grimme, S.; Antony, J.; Ehrlich, S.; Krieg, H., A consistent and accurate ab initio parametrization of density functional dispersion correction (DFT-D) for the 94 elements H-Pu. *J. Chem. Phys.* **2010,** *132*, (15), 154104.
33. Silvi, B., The spin-pair compositions as local indicators of the nature of the bonding. *J. Phys. Chem. A* **2003,** *107*, (17), 3081-3085.
34. Gillespie, R. J.; Noury, S.; Pilmé, J.; Silvi, B., An electron localization function study of the geometry of d0 molecules of the period 4 metals Ca to Mn. *Inorg. Chem.* **2004,** *43*, (10), 3248-3256.
35. Wu, M.; Yao, X.; Hao, Y.; Dong, H.; Cheng, Y.; Liu, H.; Lu, F.; Wang, W.; Cho, K.; Wang, W.-H., Electronic structures, magnetic properties and band alignments of 3D transition metal atoms doped monolayer MoS_2. *Phys. Lett. A* **2018,** *382*, (2-3), 111-115.
36. Chen, Y.-Y.; Dong, M.; Qin, Z.; Wen, X.-D.; Fan, W.; Wang, J., A DFT study on the adsorption and dissociation of methanol over MoS_2 surface. *J. Mol. Catal. A: Chem.* **2011,** *338*, (1-2), 44-50.
37. Ansari, R.; Shahnazari, A.; Malakpour, S.; Faghihnasiri, M.; Sahmani, S., A DFT study on the elastic and plastic properties of MoS_2 nanosheet subjected to external electric field. *Superlattices Microstruct.* **2016,** *97*, 506-518.
38. Rasmussen, F. A.; Thygesen, K. S., Computational 2D materials database: electronic structure of transition-metal dichalcogenides and oxides. *J. Phys. Chem. C* **2015,** *119*, (23), 13169-13183.
39. Eda, G.; Yamaguchi, H.; Voiry, D.; Fujita, T.; Chen, M.; Chhowalla, M., Photoluminescence from chemically exfoliated MoS_2. *Nano Lett.* **2011,** *11*, (12), 5111-5116.
40. Heising, J.; Kanatzidis, M. G., Exfoliated and restacked MoS_2 and WS_2: Ionic or neutral

576 species? Encapsulation and ordering of hard electropositive cations. *J. Am. Chem. Soc.* **1999,** *121*,
577 (50), 11720-11732.
578 41. Wang, Z.; Tu, Q.; Zheng, S.; Urban, J. J.; Li, S.; Mi, B., Understanding the aqueous
579 stability and filtration capability of MoS_2 membranes. *Nano Lett.* **2017,** *17*, (12), 7289-7298.
580 42. Yang, K.; Chen, B.; Zhu, X.; Xing, B., Aggregation, adsorption, and morphological
581 transformation of graphene oxide in aqueous solutions containing different metal cations.
582 *Environ. Sci. Technol.* **2016,** *50*, (20), 11066-11075.
583 43. Rathore, E.; Pal, P.; Biswas, K., Layered Metal Chalcophosphate (K-MPS-1) for
584 Efficient, Selective, and ppb Level Sequestration of Pb from Water. *J. Phys. Chem. C* **2017,** *121*,
585 (14), 7959-7966.
586 44. Zhang, W.; Shi, S.; Zhu, W.; Yang, C.; Li, S.; Liu, X.; Hu, N.; Huang, L.; Wang, R.; Suo,
587 Y., In-situ fixation of all-inorganic Mo–Fe–S Clusters for the highly selective removal of lead (II).
588 *ACS Appl. Mater. Interfaces* **2017,** *9*, (38), 32720-32726.
589 45. Liu, Y.; Liu, Z.; Gao, J.; Dai, J.; Han, J.; Wang, Y.; Xie, J.; Yan, Y., Selective adsorption
590 behavior of Pb (II) by mesoporous silica SBA-15-supported Pb (II)-imprinted polymer based on
591 surface molecularly imprinting technique. *J. Hazard. Mater.* **2011,** *186*, (1), 197-205.
592 46. Ma, S.; Chen, Q.; Li, H.; Wang, P.; Islam, S. M.; Gu, Q.; Yang, X.; Kanatzidis, M. G.,
593 Highly selective and efficient heavy metal capture with polysulfide intercalated layered double
594 hydroxides. *J. Mater. Chem. A* **2014,** *2*, (26), 10280-10289.
595 47. Manos, M. J.; Kanatzidis, M. G., Sequestration of heavy metals from water with layered
596 metal sulfides. *Chem. Eur. J.* **2009,** *15*, (19), 4779-4784.
597 48. Zhu, H.; Tan, X.; Tan, L.; Chen, C.; Alharbi, N. S.; Hayat, T.; Fang, M.; Wang, X.,
598 Biochar derived from sawdust embedded with molybdenum disulfide for highly selective removal
599 of Pb^{2+}. *ACS Appl. Nano Mater.* **2018,** *1*, (6), 2689-2698.
600 49. Sarma, D.; Islam, S. M.; Subrahmanyam, K.; Kanatzidis, M. G., Efficient and selective
601 heavy metal sequestration from water by using layered sulfide $K_{2x}Sn_{4-x}S_{8-x}$ (x= 0.65–1; KTS-3). *J.*
602 *Mater. Chem. A* **2016,** *4*, (42), 16597-16605.
603 50. Zhuang, Y.-T.; Zhang, X.; Wang, D.-H.; Yu, Y.-L.; Wang, J.-H., Three-dimensional
604 molybdenum disulfide/graphene hydrogel with tunable heterointerfaces for high selective Hg (II)
605 scavenging. *J. Colloid Interface Sci.* **2018,** *514*, 715-722.
606 51. Zhou, L.; Ji, L.; Ma, P.-C.; Shao, Y.; Zhang, H.; Gao, W.; Li, Y., Development of carbon
607 nanotubes/$CoFe_2O_4$ magnetic hybrid material for removal of tetrabromobisphenol A and Pb (II).
608 *J. Hazard. Mater.* **2014,** *265*, 104-114.
609 52. Guo, X.; Du, B.; Wei, Q.; Yang, J.; Hu, L.; Yan, L.; Xu, W., Synthesis of amino
610 functionalized magnetic graphenes composite material and its application to remove Cr (VI), Pb
611 (II), Hg (II), Cd (II) and Ni (II) from contaminated water. *J. Hazard. Mater.* **2014,** *278*, 211-220.
612 53. Yantasee, W.; Warner, C. L.; Sangvanich, T.; Addleman, R. S.; Carter, T. G.; Wiacek, R.
613 J.; Fryxell, G. E.; Timchalk, C.; Warner, M. G., Removal of heavy metals from aqueous systems
614 with thiol functionalized superparamagnetic nanoparticles. *Environ. Sci. Technol.* **2007,** *41*, (14),
615 5114-5119.
616 54. Manos, M. J.; Petkov, V. G.; Kanatzidis, M. G., $H_{2x}Mn_xSn_{3-x}S_6$ (x= 0.11–0.25): a novel
617 reusable sorbent for highly specific mercury capture under extreme pH conditions. *Adv. Funct.*
618 *Mater.* **2009,** *19*, (7), 1087-1092.
619 55. Hassanzadeh Fard, Z.; Islam, S. M.; Kanatzidis, M. G., Porous amorphous chalcogenides

620 as selective adsorbents for heavy metals. *Chem. Mater.* **2015,** *27*, (18), 6189-6192.
621 56. Fryxell, G. E.; Lin, Y.; Fiskum, S.; Birnbaum, J. C.; Wu, H.; Kemner, K.; Kelly, S.,
622 Actinide sequestration using self-assembled monolayers on mesoporous supports. *Environ. Sci.*
623 *Technol.* **2005,** *39*, (5), 1324-1331.
624 57. Wander, M. C.; Clark, A. E., Hydration properties of aqueous Pb (II) ion. *Inorg. Chem.*
625 **2008,** *47*, (18), 8233-8241.
626 58. Zhang, Q.; Yang, Q.; Phanlavong, P.; Li, Y.; Wang, Z.; Jiao, T.; Peng, Q., Highly efficient
627 lead (II) sequestration using size-controllable polydopamine microspheres with superior
628 application capability and rapid capture. *ACS Sustain. Chem. Eng.* **2017,** *5*, (5), 4161-4170.
629 59. Yan, Z.; Fu, L.; Yang, H., Functionalized 2D clay derivative: hybrid nanosheets with
630 unique lead sorption behaviors and interface structure. *Adv. Mater. Interfaces* **2018,** *5*, (4),
631 1700934.
632 60. Wang, Z.; von dem Bussche, A.; Qiu, Y.; Valentin, T. M.; Gion, K.; Kane, A. B.; Hurt, R.
633 H., Chemical dissolution pathways of MoS_2 nanosheets in biological and environmental media.
634 *Environ. Sci. Technol.* **2016,** *50*, (13), 7208–7217.
635 61. Pieper, K.; Martin, R. L.; Tang, M.; Walters, L.; Parks, J.; Roy, S.; Devine, C. L.;
636 Edwards, M. A., Evaluating water lead levels during the Flint Water Crisis. *Environ. Sci. Technol.*
637 **2018,** *52*, (15), 8124-8132.
638 62. Yang, X.; Li, J.; Liang, T.; Ma, C.; Zhang, Y.; Chen, H.; Hanagata, N.; Su, H.; Xu, M.,
639 Antibacterial activity of two-dimensional MoS_2 sheets. *Nanoscale* **2014,** *6*, (17), 10126-10133.
640 63. Alam, I.; Guiney, L. M.; Hersam, M. C.; Chowdhury, I., Antifouling properties of two-
641 dimensional molybdenum disulfide and graphene oxide. *Environ. Sci. Nano* **2018,** *5*, (7), 1628-
642 1639.
643